IEEE Access
Multidisciplinary | Rapid Review | Open Access Journal

Received January 22, 2021, accepted January 24, 2021, date of publication February 1, 2021, date of current version February 8, 2021.

Digital Object Identifier 10.1109/ACCESS.2021.3056050

Radial Basis Function Neural Network for the Evaluation of Image Color Quality Shown on Liquid Crystal Displays

FELIPE ARIAS DEL CAMPO, OSSLAN OSIRIS VERGARA VILLEGAS, (Senior Member, IEEE), VIANEY GUADALUPE CRUZ SÁNCHEZ, HUMBERTO DE JESÚS OCHOA DOMÍNGUEZ, (Member, IEEE), AND MANUEL NANDAYAPA, (Member, IEEE)

Instituto de Ingeniería y Tecnología, Universidad Autónoma de Ciudad Juárez, Chihuahua 32310, México

Corresponding author: Osslan Osiris Vergara Villegas (overgara@uacj.mx)

ABSTRACT The color quality of an image shown on a liquid crystal display (LCD) can be measured with a spectroradiometer; however, this instrument is expensive, work under controlled illumination conditions with an artificial source of light, and measurements take a long time. A spectroradiometer returns measurements of wavelength or CIE color space. A low-cost and fast alternative consists of using a digital camera that outputs RGB measurements. Unfortunately, comparisons between measurements obtained with both instruments cannot be performed; hence, conversion equations must be used. The main problem is that equations do not consider the effects caused by the camera lens, sensor variations, and configurable parameters such as gain and the exposure time. This paper proposes the architecture of a radial basis function neural network (RBFNN) to measure the image color quality displayed by an LCD using a digital camera. The RGB values acquired with a camera are used as inputs to the RBFNN. The output predicted the luminance and chromaticity components in the CIExyY color space and included the corrections to the lens and camera parameters. First, the RBFNN topology is explained, including the calculation of the number of neurons in the hidden layer, and the definition of the dispersion centers and their associated spread. Next, the experiments related to RGB color space reconstruction and conversion from RGB to CIE are presented. The proposed approach was tested on a real automotive scenario. The results obtained were similar to those measured with the spectroradiometer with an accuracy of 93.3%. Moreover, the results remained within limits established by the six-sigma methodology.

INDEX TERMS Liquid crystal display, radial basis function neural network, digital camera, spectroradiometer, RGB, CIE.

I. INTRODUCTION

The use of display technologies has become indispensable in the modern world. Currently, liquid crystal displays (LCD) are dominant technology due to their size, low-drive voltage, and low-power consumption, encountering applications in computer monitors, televisions, tablets, smartphones, among others [1]. The introduction of digital displays in the automotive industry occurred in the middle of the 70s. Since then, the display market for automotive applications has significantly evolved [2], [3]. Now, LCDs are almost standard accessories in the design of modern automobiles to provide information, assistance, control, and entertainment to the driver [4]. The possibility of displaying different information in the same place helps save space and allows the customization of the information according to the user preferences or needs [5].

The manufacturing process of LCDs has many optical challenges, including the detection of defect regions, pixel failure (always off or on), mura (a non-uniformity distortion, in luminance or color), intensity, uniformity, and abnormal reproduction of colors (perceivable regional color variations) [6], [7]. The task of error detection can be carried out either visually or with specialized inspection

The associate editor coordinating the review of this manuscript and approving it for publication was Jeon Gwanggil.

equipment. The visual inspection method can be applied in most cases, but it is costly, time-consuming, non-repeatable, human dependent, and subject to the inspector's perception and criteria. In contrast, errors that cannot be perceived by human eyes can be detected using specialized equipment, and the measurements obtained are repeatable and consistent. However, the equipment can be expensive, sometimes it is not possible to reach the target object with the measurement instrument, and the time employed to obtain results can be long [8].

Defects such as pixel failure, intensity, and non-uniformity can be detected using digital cameras. The main idea is to capture an image and then analyze it with specialized algorithms. The camera gives images composed of three planes, Red, Green, and Blue (RGB). The color of a pixel is generated by the combination of each color plane intensity using 8-bits values. However, the verification of the color of an image displayed in an LCD cannot be carried out by a human, because nobody can guarantee that colors perceived by different inspectors are the same [9]. Therefore, this task requires more specialized equipment such as a spectroradiometer [10].

A spectroradiometer measures the wavelength and amplitude of the light emitted by a light source, and assures accurate and repeatable measurements of color, luminance, and spectral radiance information. Also, it preserves the spatial relationship of measurements across the display, which is required for measuring spatial variations. The measures obtained can be represented with different units including the light wavelength, amplitude, CIExyY, CIE XYZ, and CIE $L^*a^*b^*$ [11].

The use of a spectroradiometer to detect color defects in production lines is an expensive solution. Today, a spectroradiometer could cost more than 50,000 dollars. Also, the controlled conditions to use it must be considered, which further increases the cost of the manufacturing test equipment. Therefore, a lower-priced solution, like the use of a digital camera, is desirable. However, before implementing this solution, several problems must be addressed. For example, the camera cannot offer the spectral accuracy of a spectroradiometer, the image is captured in RGB space (however, sometimes it is transformed into a grayscale image), and the acquired images are subject to variations in color and intensity caused by the camera location and lens, to mention a few.

A color conversion must be conducted to compare the measures obtained with a camera to those obtained with a spectroradiometer. In the literature, equations to convert from RGB to CIExyY or CIE $L^*a^*b^*$ color spaces have been proposed. Nevertheless, the equations can only be applied to convert the color after it has been digitized [12]. Several parameters affect the measurements when a camera is used for color digitalization, including the lens, angles, digital gain, exposure time, gamma, brightness corrections, among others. Consequently, the values obtained by the conversion from RGB to CIExyY will be different from the values obtained with a spectroradiometer. Hence, it is almost impossible to perform comparisons.

This research was motivated by two main issues. First, to present a solution to an actual problem related to the cost of the equipment required to measure color in a massive production environment, and second, but not least important, the interest in bring closer academic research to the actual manufacturing world. The scientific developments sooner or later reach a maturity level that ends in materializing an artifact that satisfies a real necessity. However, the researchers often limit their work to the academic scenarios, stopping short on the actual implementation of their work. Thus, this work intends to provide a real implementation of a concept that is known to be used to solve many problems but, as far as we found, it has had a short presence in the engineering world.

Accordingly, in this paper, a proposal to solve the problem of accurately converting the RGB values acquired with a digital camera to CIExyY color space values obtained with a spectroradiometer is presented. A radial basis function neural network (RBFNN) is used to perform the conversion and to compensate for the variations in the environmental conditions, the camera parameters, the camera lens distortion, and the effect of its physical restrictions. In other words, we propose an innovative method to characterize complex systems eliminating the need to define mathematical models to compensate environmental factors by using the RBFNNs. In the manufacturing industry, where the proposed solution was implemented, the quality measurement of the colors displayed in an LCD was done using a spectroradiometer, which implies high costs and long inspection times. In contrast, our proposal is less expensive and achieves competitive results in a real scenario by using less time. To the best of our knowledge, using RBFNNs has not previously been reported to solve the aforementioned problem.

The main contributions of this paper are as follows:

- We propose an automatic method that uses RBFNNs to convert RGB values to CIExyY by compensating the environmental variations.
- We demonstrate how the RGB images acquired with a digital camera are used to obtain similar color measures to those obtained with a spectroradiometer at a lower cost.
- We present the design of a configurable scenario to acquire color measurements with a digital camera.
- We implement our proposal in a real automotive scenario, obtaining competitive results.

The rest of the paper is organized as follows. In Section II, the literature review, the theoretical framework of RBFNNs, and the explanations about how to use a digital camera for colorimetry purposes are presented. The research methodology is explained in Section III. The experiments and results are provided in Section IV. Finally, the conclusions and further work are presented in Section V.

II. BACKGROUND

In this section, the analysis and comparison of the related literature works is presented. Also, a theoretical explanation about how an RBFNN operates is introduced. Finally, an explanation of how to use digital image-based colorimetry is offered.

A. RELATED WORK

A search was conducted to detect related work in the period 2010-2020. The search included papers published in journals and conferences, and the engines employed were the typical for sciences, including IEEE, Springer, ACM, Willey, and Taylor & Francis.

Two main branches were detected according to the search. The first one uses the RGB colors acquired with a digital camera to measure concentrations in solutions or materials in the environment. The output of this kind of system was not a color value. Instead, an absorbance/presence measurement was obtained [13]–[15]. The other branch uses the RGB measurements to conduct color plane transformations. This kind of system frequently transforms values into the CIE color plane intending to compare the results with those obtained with a spectroradiometer or similar equipment [9], [11], [16].

From the literature perusal, only a few papers that use a camera to measure color in the same way that can be performed by using a spectroradiometer were detected. However, one work of the other branch was first discussed because it was the only one that uses a neural network to solve the problem. Each work is discussed below.

Bang-iam *et al.* [13] employed a backpropagation neural network to detect proteins in latex materials (natural rubber and gloves). The Lowry method was used to create eleven solutions with different concentrations to determine the total protein level. The authors built a closed box where the illumination LEDs, the camera, and the sample holder were located. The absorbance of the solutions was measured with an UV–Vis spectrophotometer and the RGB values with the camera-based system. An accuracy of 89.8% was obtained as a result of the experiments.

The work by Sanmartín *et al.* [16] describes the process to calibrate a digital camera to be used as a colorimeter. The camera was used to measure the color of granite artworks. The low chroma values of the granite were reported as the main challenge. The problem was solved with a linear model using multiple measurements taken with a spectrophotometer and a camera. The measurements obtained with the camera were converted from RGB to the CIE $L^*a^*b^*$ color space. The results showed a difference of 1.32 (using the color similarity method $\Delta E\star_{ab}$) between the values obtained with the proposed model and the values obtained with the direct transformation from RGB to CIE $L^*a^*b^*$.

A systematic framework that uses high-dynamic-range (HDR) imaging to measure subtle color defects in flat panel displays (FPD) was presented in the work of Nam *et al.* [9]. The core of the proposal was a method to convert the device-dependent HDR RGB signals into device-independent color coordinates of CIE *XYZ*. First, the camera was characterized. Second, an FPD was selected, and a total of 24 color patches were displayed in it. Then, each patch was sequentially captured with a spectroradiometer and the camera. Also, the images captured with the camera were combined into the HDR radiance map. Finally, a linear transformation that converts RGB camera signals into CIE *XYZ* values was performed. A reference image of a well finished FPD product was used for comparisons. Contrast sensitivity functions were used to compute the visual difference of color defects at various frequency levels. The accuracy obtained was 95.61%.

Notermans and Cohen [11] presented an instrument that combined the strengths of a spectrometer and a high-quality camera to provide rapid and reliable measurements of color displays. The spectrometer collected the light from its field of view and provided a measurement of intensity as a wavelength function. Then, the data was processed to recover the CIE *XYZ* values. Simultaneously, a CCD camera acquired an RGB image. The region captured with the camera corresponded to the area sampled by the spectrometer. The image was processed to recover the sum of the RGB values. The ratio of the two measurements yielded a conversion factor. Unfortunately, no information about the tests and results obtained was offered.

Table 1 shows a summary of the literature work.

As it can be observed from Table 1, two works used a spectroradiometer, one used a spectrometer, and the other used a spectrophotometer for comparison purposes. The largest camera resolution was 16 MP, followed by 10, 6.6, 5, and 4 megapixels. One work verified proteins, one granite artwork, two FPDs, and one LCDs. The last four works performed conversions to CIE color space. Our proposal is the third one that inspected most images. None of the works employed a neural network to solve the color conversion. Note that the lowest and highest accuracy are 76% and 95.61%, respectively.

B. RADIAL BASIS FUNCTION NEURAL NETWORKS: BRIEF THEORETICAL BACKGROUND

One of the major disadvantages of a backpropagation neural network (BPNN) is that the training speed decreases as the number of layers and neurons increases. It is also challenging to determine the most suitable architecture to solve a problem [17]. To overcome these issues, Powell [18], [19] introduces the RBFNN as a feedforward architecture with one hidden layer that uses a radial basis function (RBF) to process input data.

RBF networks are gaining popularity due to many advantages compared to other types of artificial neural networks, which include a good response for patterns not used for training, better approximation capabilities, simpler structure, easy design and training, tolerance to input noise, faster learning algorithms, and online learning ability. Moreover, an RBFNN can characterize complex functions by providing only the

TABLE 1. Summary of the works analyzed in the literature review.

Authors	Instrument	Camera	Lens	Part verified	Color space conversion	Algorithm	Images tested	Accuracy
Bang-iam et al. (2013) [13]	Spectrophotometer	4 MP Microsoft HD-5000	Plastic	Protein	Absorbance	Backpropagation	11	89.8%
Sanmartín et al. (2014) [16]	Colorimeter	6.6 MP PixeLINK PL-A782	Fujinon CF50HA-1 50-mm	Granite artworks	CIE $L^*a^*b^*$	Target based characterization	222	76%
Nam et al. (2016) [9]	Spectroradiometer	5.0 MP PointGrey Grasshopper2	Pointgray 35-mm	Flat Panel Display	CIE XYZ	Color matching functions	N/A	95.61%
Notermans and Cohen (2016) [11]	Spectrometer	16 MP Bobcat	N/A	Flat Panel Display	CIE XYZ	Measurement ratio	4	N/A
Our Proposal (2020)	Spectroradiometer	10 MP iDS UI-5490SE-C	KOWLM8JC10M 8-mm	Liquid Crystal Display	CIExyY	RBFNN	10	93.3%

training sets, avoiding a complex analysis on the system to approximate [20]. The simple topological structure with the ability to characterize complex functions and the fast learning were critical features considered to select the RBFNN as a competitive method to solve the problem stated in this paper.

The RBFNN consists of three layers: the input layer, the hidden layer, and the output layer. Each layer is fully connected to the next, and there is no bias term [21], [22]. The input neurons x (feature vector to be classified), also called identity neurons, are represented by the symbol shown in Fig. 1a. The neurons in the hidden layer use RBF to process the inputs. Each neuron consists of an RBF centered at the point c in the input space. The average distance between all points of a N-dimensional feature vector to c is known as the Gaussian activation function. In general, the closer the input vector is to the center vector of an RBF neuron, the higher is the value at the output of the neuron. The name RBF is used because the value of the function is the same for all points that are at equal distance from the center. The symbol to represent hidden neurons is shown in Fig. 1b. The output neurons supply the response from the network to the outside world; its symbol is shown in Fig. 1c. These neurons use a weighted sum as a propagation function and the identity as the activation function [23].

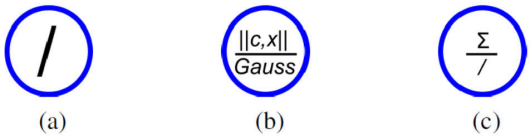

FIGURE 1. Neurons of the RBFNN: (a) Input, (b) RBF, and (c) Output [23].

An example of the RBFNN architecture with three neurons in the input layer, four neurons in the hidden layer, and two neurons in the output layer is shown in Fig. 2. Observe that the connections from the input to the hidden neurons are not weighted.

The most popular RBF is given in Equation (1).

$$\varphi_i(||x - c_i||) = exp\left(-\frac{||x - c_i||^2}{2\sigma_i^2}\right) \tag{1}$$

where x is the input vector, $||\cdot||$ is the Euclidean norm, c_i is the center of the *ith* RBF unit, and σ is the spread of the RBF.

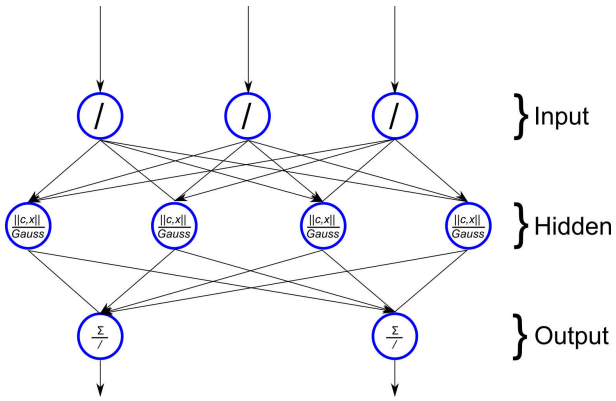

FIGURE 2. Architecture of a traditional radial basis function neural network.

Typically, the Gaussian function φ is selected with σ being the spread parameter. Fig. 3 shows two Gaussian functions, centered at zero with $\sigma = 20$ and $\sigma = 10$.

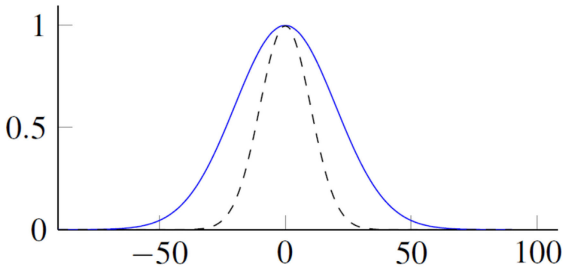

FIGURE 3. Two bells-shaped obtained with two Gaussian functions, using $\sigma = 20$ (solid line) and $\sigma = 10$ (dashed line).

The *jth* output node of the output layer is defined as the *jth* hypothesis $h_j(x)$ and it is defined in Equation (2).

$$h_j(x) = \sum_{j=1}^{n}(\varphi_i(x)W_{ij}) \tag{2}$$

where n is the number of activation functions in the hidden layer and W_{ij} the weights from the hidden to the output layer.

For a data set of m examples defined by $\{(x_1, y_1), (x_2, y_2) \cdots (x_m, y_m)\}$ where the pair (x_i, y_i) corresponds to the *ith* input example x_i and the corresponding ground truth y_i. The learning can be formulated as the minimization of the cost C defined by the sum-squared-error function

of Equation (3).

$$C = \frac{1}{2m}\sum_{k=1}^{m}(y_k - h(x_k))^2 \tag{3}$$

In summary, the RBFNN is a universal approximator much faster and simpler than the Multilayer Perceptron (MLP).

C. DIGITAL IMAGE-BASED COLORIMETRY

The spectroradiometer is the most accurate tool to measure the spectral information of a light source, and consequently, to measure pure color. Conversely, a high-resolution camera can quickly measure the light intensity displayed by a source in a single shot. Nevertheless, the cameras only detect changes in light intensity (brightness) and not in color [24].

A traditional chamber used to measure the color of an object employing a digital camera is shown in Fig. 4. In its ideal configuration, shown in Fig. 4a, the camera is aligned at 90°, pointing directly to the center of the object. The line that passes through the camera center represents an imaginary axis perpendicular to the center of the object. However, when the chamber is designed applying industry standards and guides (ergonomic regulations, manufacturing floor footprints, equipment standardization guides), it is common that the camera needs to be shifted and sometimes rotated. Therefore, the imaginary center line does not pass through the camera center. The camera should be placed outside the chamber to ensure the ideal configuration, as it is shown in Fig. 4b.

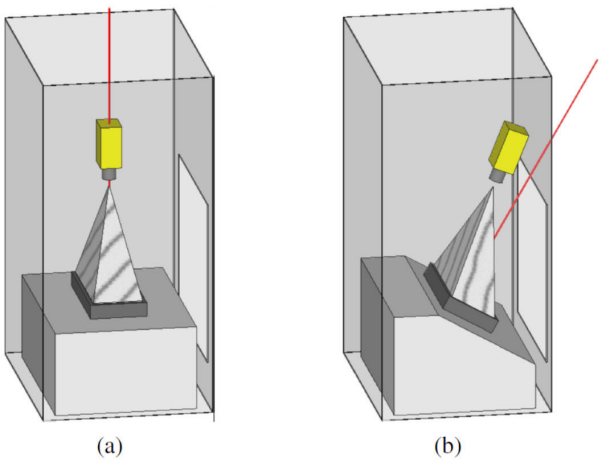

FIGURE 4. Design of the tester for object inspection: (a) Ideal design, and (b) Real design.

The measurement process comprises four elements that have a different impact on the computed color values: (i) the object placed on a nest to ensure the same position for repeatability purposes; (ii) the measurement instrument, in this case, the digital camera and its lens; (iii) the camera distance and location to acquire the entire object; and (iv) the configurable camera parameters, such as the color channel gain, exposure, and gamma correction.

The camera lens is manually adjusted to get the correct focus and iris aperture. The goals are to obtain an image with the best clarity and to avoid the saturation of the camera imaging sensors when the brightness of the display is set too high (during the test, the display needs to be verified using high and low-brightness settings).

Three factors need to be considered to select the best location of the camera. First, the test equipment must be designed to be reused for different products when the original one is no longer in production. The camera does not have a fixed location; it must have the possibility of being manually adjusted in three axes (yaw, pitch, and row). Second, the tester must be planned to inspect objects with different sizes. Also, the mechanical restrictions for connectors, labels, guides, and shapes must be considered. All this implies that the geometric center of the object, in relation to the camera, may change between models. Third, design restrictions related to space and ergonomic guides must be considered. For instance, if the camera needs to be located in a position where it can see the entire object, then it may not be placed or oriented in the ideal position (pointing to the middle axis of the display).

The camera parameters such as gain, exposure time, and white reference can be reconfigured using software commands. Once the camera, lens, and related parameters are adjusted, the settings remain constant, and the inspection process starts.

To create color images, red, green, and blue filters are placed over individual pixels on the image sensor. Afterward, some interpolation is used to compute the color of each pixel for the digitalized image. The calculation is done by combining the light intensity captured directly from one color (the light intensity after one color filter) with the other two colors captured by the pixels around it.

When an RGB image is acquired with the camera, it is processed in a computer using specialized software routines. Also, the process of color conversion is conducted. The RGB image acquired with a camera depends on the system parameters. As a consequence, a direct transformation from RGB to CIE cannot be conducted. A camera characterization process is needed to define the mapping between RGB and the device-independent color space. The characterization is used to predict the camera response given an input energy spectral distribution [25].

The color conversion transforms the RGB color measured by the camera (Fig. 5a), to the bi-dimensional (x, y) CIE 1931 color space used by the spectroradiometer (Fig. 5b). However, other possible units like the CIE *Luv* color space or the wavelength could be used. Finally, a comparison of the color values obtained with the camera and the spectroradiometer is performed to have an insight about the accuracy measured with the camera.

III. MATERIALS AND METHODS

For training the network, the R, G, and B components are taken as the input parameters, and the luminance (Y), and chromaticity coordinates (x and y) from the CIExyY are the output parameters which are compared with the measurements from the spectroradiometer. In addition to the color

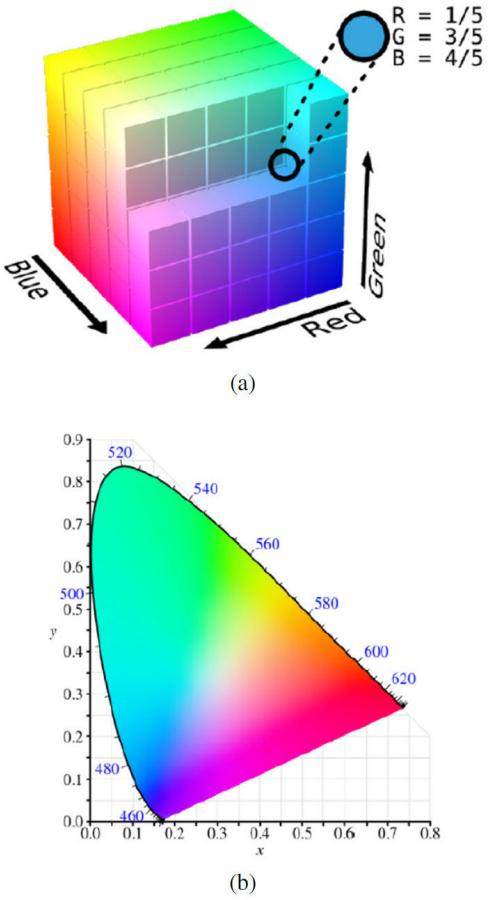

FIGURE 5. Color space conversion: (a) Three-dimensional space (RGB) measured with the camera, and (b) Bi-dimensional space (x, y) CIE 1931 xyY measured with the spectroradiometer.

transformation, the model includes the variables related to the equipment design (distance, position of the camera, and field of view) and the camera parameters, like gain, sensitivity, and lens focus.

In this section, the processes to obtain the test images, to measure the ground truth color values with the spectroradiometer, to measure color with the camera, to use the RBFNN and to establish a color similarity error are explained.

A. TEST IMAGES

A set of 125 uniform color, solid filled images to be displayed in the LCD was generated utilizing a windows application. The RGB color to be displayed in the LCD was generated by changing each of the three values of the color intensity (Red, Green, and Blue). Even though the full range is from 0 to 255, only a range from 0 to 128 tones was considered to avoid the saturation[1] of the camera color sensors. The color range was divided into four intervals (0-31, 32-63, 64-95, 96-128).

For example, the color to be displayed could be the black (0,0,0). If the R-value is increased, the next color is (32,0,0). If a G-value (0,128,0) is generated, then by stepping the B-value, the next color is (0,128,32).

Finally, a total of 70 images were randomly chosen from the generated set of 125. The resulting set was divided into 60 images for training and 10 for testing ($\approx 14\%$) according to the Guyon's rule [26].

[1]When the sensors are exposed to a very bright color, the captured image will be fully white.

B. MEASUREMENT OF THE GROUND TRUTH COLOR VALUES WITH THE SPECTRORADIOMETER

The color reference values or ground truth in the CIE 1931 xyY space were measured in a manufacturing laboratory with an OL 770-DMS Gooch & Housego spectroradiometer with a 610 telescopic lens. The spectroradiometer was mounted on a fixed base, as it is shown in Fig. 6. The LCD was mounted on three axes adjustable fixture at a distance of 50 cm from the spectroradiometer. The measurements were taken on a 12" LCD.

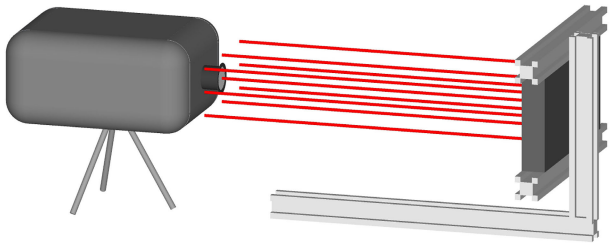

FIGURE 6. Conceptual view of the spectroradiometer setup.

The 70 images in the data set were sequentially displayed in the LCD. For each image, nine acquisitions were taken, each located in different coordinates (points), as shown in Fig. 7.

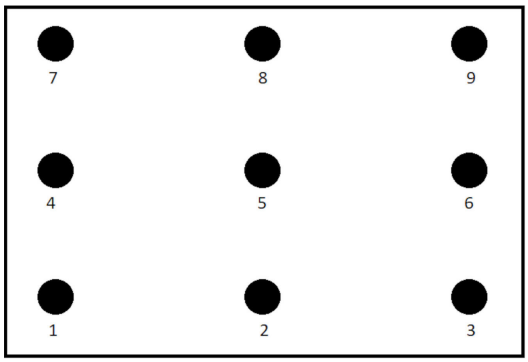

FIGURE 7. Location of the color measurement points on the LCD.

The measurement process started by moving the first point of the LCD in the spectroradiometer field of view. Then, the first measurement is taken. Afterward, the LCD is moved to the next location to measure the second point. The process is repeated until the nine points are measured. The LCD movement allowed the measure of each of the nine points with the same visual angle concerning the spectroradiometer.

Seven parameters were measured at each point: luminance (cd/m^2); coordinates in the CIE 1931 xyY color space (x, y);

color components in the *Luv* color space (u', v'), dominant wavelength (*nm*) and saturation (*s*). Measurements at each point are averaged to obtain the total reference value. The results are stored in a file, including the reference between the color displayed and the measured value.

C. MEASUREMENT OF THE COLOR VALUES WITH THE CAMERA

The tester was simulated using a chamber to create a dark space. The LCD was placed at one end inside the chamber, and the camera at a distance of 40 cm, as it can be observed in Fig. 8. The perpendicular display plane is pointed about 10 degrees relative to the camera lens vision axis, to resemble the conditions employed to measure the ground truth. The camera used was a digital Gigabit Ethernet iDS model UI-5490SE-C with a Kowa 2/3″ 10 megapixels 8.0mm lens (model KOWLM8JC10M).

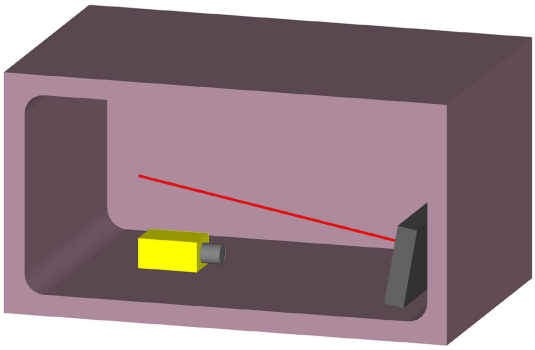

FIGURE 8. The chamber containing the LCD and the camera.

After the camera and lens are aimed and adjusted, the same sequence order of images measured with the spectroradiometer is displayed on the LCD. The RGB values of each acquired image, are averaged to obtain a single RGB color value. The measured values are stored in a file and used as the input examples to train the RBFNN.

D. RBFNN MODEL

The color conversion is performed using an RBFNN. The goal is to approximate the network functions to convert the RGB color measurements, taken with the camera, to the values measured with the spectroradiometer in the CIE 1931 *xyY* color space.

The centers are distributed over the space of the function, as it can be observed in Fig. 9a. During the training, the distance of each point of the function to each neuron center is learned (Fig. 9b).

When an RBFNN is used to characterize a function in a bi-dimensional space, it can be visualized as a circle (Fig. 10a), where the distance between the center and a point (the radius) drives its activation. In contrast, when the characterized function is defined in three-dimensional space, it can be represented as a sphere (Fig. 10b).

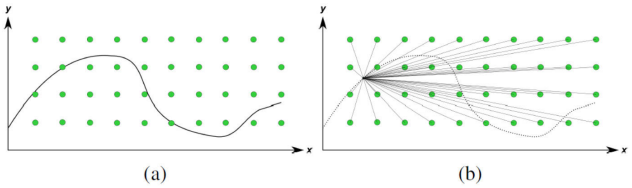

FIGURE 9. Conceptualization of an RBFNN to learn an arbitrary function: (a) The neuron centers are distributed over the function space, and (b) The model is trained to learn the function by using the distance between each data point and each neuron's center.

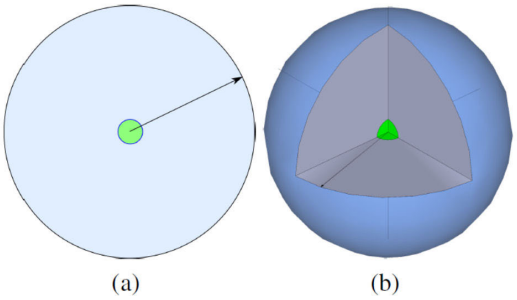

FIGURE 10. Representation of neurons: (a) The 2D case (circle), and (b) The 3D case (sphere).

Because the RGB color space has three components, the input data to the network is visualized as a 3D space, where each color component is aligned with an axis. Originally, the values that each component can take goes from 0 to 255. However, the generated images had a maximum value of 128 for each channel. Due to the radial function, each neuron of the network was represented as a sphere (3D space).

The neuron center is placed in a three-dimensional space. The neuron location is defined by the range of the color and the number of neurons placed on each axis (n). The value of the range is used to define the area covered by the neurons. For interpolation, this value should be in the range of the color space (0 to 255). However, the value can be extended to cover a volume that exceed the range of the color space. The experiments showed that by covering a bigger volume, even if it is empty, helped to improve the network interpolation capability. The center of the entire network should be the same center of the volume defined by the color space.

An example of the distribution of the neurons for the red color is shown in Fig. 11. The horizontal and vertical axis represents the red color plane. The neurons are evenly distributed in the entire surface, as shown in Fig. 11a. Then, each axis is divided by $n-1$, where n is the number of neurons to be located on each edge (minimum 2). If $n = 2$, then two neurons will be placed on each edge.

It is worth noting that two edges share neurons in the vertex. The RBF σ value is set to represent the 90% of the distance between the centers (Fig. 12), and they are considered the core neurons. The number of core neurons is defined as n^3. Therefore, when $n = 2$, two neurons are placed in each vertex of the 3D space, for a total of 8 core neurons.

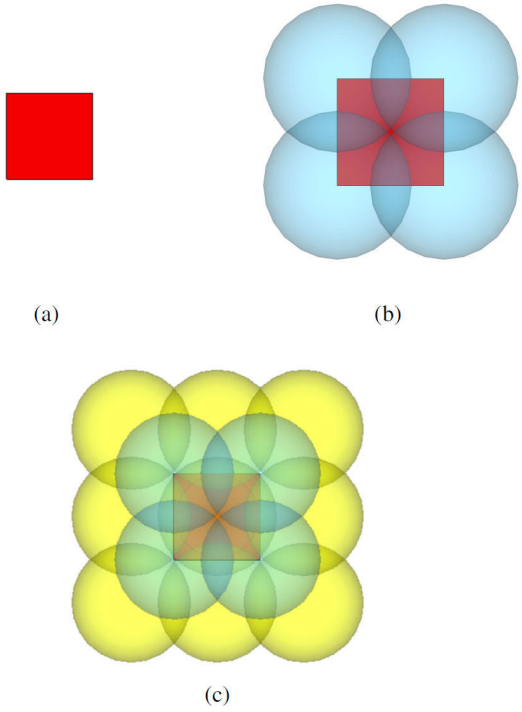

FIGURE 11. Neuron centers distribution: (a) Red color plane where the neurons are evenly distributed, (b) Neurons placed on each edge, and (c) Additional neurons added to cover the gaps.

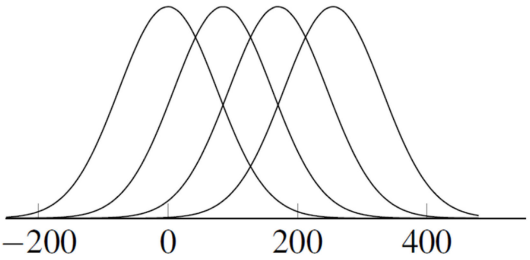

FIGURE 12. Gaussian distribution with an overlap of 90% of the distance between the neuron centers.

The center of the plane is located relatively far from the influence of the core neurons, as it is shown in Fig. 11b. By making an analogy between neurons and a light source, it is possible to think that the middle point between two light rays will receive less light. Hence, to make the illumination more even, additional light rays need to be added in the middle. Therefore, to improve the interpolation capability of the network, additional neurons are added to cover the space (fill the gaps) between the sphere of influence, including one layer in the outside. An example of this is shown in Fig. 11c.

The Euclidean distance of the input vector x to the hidden neuron H_m is calculated with Equation (4).

$$distance = \sqrt{\sum_{i=1}^{3}(X_i - H_{m_i})^2} \tag{4}$$

where m is the *mth* neuron in the hidden layer. The calculated value of the distance is passed to the Gaussian activation function, given by Equation (5), which is similar to Equation (1).

$$activation = exp\left(-\frac{distance^2}{2\sigma_i^2}\right). \tag{5}$$

When the model was tested, it was observed that an additional layer around the original core neurons helped to improve the network training, the convergence and the approximation. The total number of additional neurons is calculated as $(n+1)^3$. Therefore, the complete RBFNN is made of $(n^3) + (n+1)^3$ neurons in the hidden layer. The minimum value of $n = 2$ is established because it gives the smallest number of neurons required to cover the cubic space. In contrast, the maximum value of $n = 4$ is established because with larger values the network does not converge.

All the neural networks have associated variables, also called hyperparameters, which determine the network architecture (topology) and how it is trained [27].

A summary of the hyperparameters related to the proposed RBFNN topology is shown in Table 2. The distribution of the neurons in the three-dimensional space is done in two blocks. The first is based on the color range for which the model is trained, and this set is labeled as *color neurons*. The second block of neurons named *fill neurons*, is added to improve the model accuracy by filling the gaps between the color neurons. The two defined blocks of neurons are just for conceptualization. When the model is trained or used to evaluate a real-world value, all the neurons in the hidden layer are processed in the same way.

TABLE 2. Hyperparameters of the proposed RBFNN.

Hyperparameter	Value
Color neurons	
Axis range	0 to 120
Red axis step	40
Green axis step	40
Blue axis step	40
Hidden layer total nodes	64
Fill neurons	
Axis range	-20 to 140
Red axis step	40
Green axis step	40
Blue axis step	40
Hidden layer total nodes	125

On the other hand, a summary of the hyperparameters related to RBFNN training is shown in Table 3. The values of the hyperparameters are tuned through the classical grid search [28].

E. THE COLOR SIMILARITY ERROR FUNCTION

The colors are compared using a reference to determine their similarity. The comparison between two colors could be described using adjectives. However, the necessity to accurately distinguish the color similarity detonated the proposal of formal comparison methods [29].

TABLE 3. Hyperparameters for training the proposed RBFNN.

Hyperparameter	Value
Inputs	3
Outputs	3
Learning rate	0.09
Stop error threshold	1
Training timeout	1 hour
Beta	27

In the twenty-first century, the color spaces known as CIELAB and CIELUV were proposed as a recommendation to quantify and judge color [30]. In 1984, the Colour Measurement Committee (CMC) of the Society of Dyes and Colourists of Great Britain published the color difference method known as ΔE_{CMC} [31].

The ΔE_{CMC} method included the parameters l and c, to define factors for lightness and chroma. Hue (H) was defined as a constant with a value of 1. The default ratio of l and c is 2:1, allowing twice the lightness difference than chroma. The human eye can detect changes in chroma better than in lightness. The method calculates the dissimilarity between two colors in the *Lab* color space. Therefore, a reference color (L_1, a_1, b_1) and a sample color (L_2, a_2, b_2) are used. The $\triangle E$ value is given by:

$$\triangle E_{CMC} = \sqrt{\left(\frac{\triangle L}{lS_L}\right)^2 + \left(\frac{\triangle C}{cS_C}\right)^2 + \left(\frac{\triangle H}{S_H}\right)^2}, \quad (6)$$

where $\triangle L$, $\triangle C$ and $\triangle H$ are the differences of the two colors being compared, and defined by the Equations (7), (8) and (11) respectively.

$$\triangle L = L_1 - L_2 \quad (7)$$

$$\triangle C = C_1 - C2 \quad (8)$$

where:

$$C_1 = \sqrt{{a_1}^2 + {b_1}^2} \quad (9)$$

$$C_2 = \sqrt{{a_2}^2 + {b_2}^2} \quad (10)$$

$$\triangle H = \sqrt{\triangle a^2 + \triangle b^2 - \triangle C^2} \quad (11)$$

where:

$$\triangle a = a_1 - a_2 \quad (12)$$

$$\triangle b = b_1 - b_2 \quad (13)$$

S_L, S_C and S_H are additional functions given by the Equations (14), (15) and (16) respectively.

$$S_L = \begin{cases} 0.511, & \text{if } L_1 < 16. \\ \dfrac{0.040975\, L_1}{1 + 0,01765 L_1}, & \text{if } L_1 \geq 16. \end{cases} \quad (14)$$

$$S_C = \frac{0.0638 C_1}{1 + 0.0131 C_1} + 0.638 \quad (15)$$

$$S_H = S_C(FT + 1 - F) \quad (16)$$

where:

$$T = \begin{cases} 0.56 + |0.2\cos(H_1 + 168°)|, & \text{if } 164° \leq H_1 \leq 345°. \\ 0.36 + |0.4\cos(H_1 + 35°)|, & \text{otherwise.} \end{cases} \quad (17)$$

$$F = \sqrt{\frac{{C_1}^4}{{C_1}^4 + 1900}} \quad (18)$$

$$H = \arctan\left(\frac{b_1}{a_1}\right) \quad (19)$$

$$H_1 = \begin{cases} H, & \text{if } H \geq 0. \\ H + 360°, & \text{otherwise.} \end{cases} \quad (20)$$

IV. EXPERIMENTS AND RESULTS

Two experiments were conducted to evaluate the performance of the proposed RBFNN. The first was used to verify the capability to reconstruct the entire RGB color space and the second to test the color space conversion from RGB to CIE 1931 xyY.

A. RGB COLOR SPACE RECONSTRUCTION

The RBFNN was trained with three sets of reference values, including 27, 60, and 200 colors, respectively. The selection of the training sets size was made, considering that 27 is close to the actual number of available samples at the first prototype stages in a typical development cycle of a new LCD application. A set size of 60 is small enough to fit in the slot of time for which the spectroradiometer was available for utilization. Finally, 200 is chosen to verify if a larger set size improve the results.

The reference values for each set where randomly chosen from a total of 16,777,216 (2^{24}) possible values in the RGB color space. Therefore, an input $R_1G_1B_1$ yields an output $R_2G_2B_2$ in such a way that $R_1G_1B_1 = R_2G_2B_2$. To visualize the colors in the 3D space, the value of each color component was mapped as a coordinate value in x, y, and z axis, respectively. An example of a 3D representation of the set with 200 random samples is shown in Fig. 13. It should be noted that the axis ranges goes from 0 to 255.

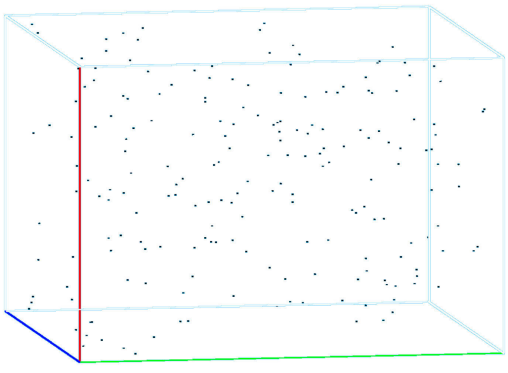

FIGURE 13. 3D localization of 200 sample colors randomly generated.

The proposed algorithm 1 generates a wire cage cube (3D grid) with a configurable number of divisions in two of the three axes. Also, it was used to evaluate the performance of the RBFNN trained. The complete wire cage was produced by changing the third axis in steps of one (from 0 to 255). Each value was used as the input for the RBFNN, and the returned value was expected to be the same. The color difference (error) between the input and output was evaluated with the ΔE_{CMC} method. The accuracy is dependant of the capability of the RBFNN to interpolate the entire 3D color space.

An example to evaluate the color red is described in Algorithm 1. Nevertheless, a similar process was used to evaluate the green and blue colors. The difference is carried out by switching the order of color components in the loop, and by changing two colors with big steps and the other color with one step. The result obtained from algorithm 1 represents the average estimated error of all the interpolated points. Ideally, the value should be zero, when all the colors are identical. Any value less than two indicates that both colors cannot be visually differentiated.

The grid obtained by using three divisions (85 steps) in the blue and green axis, with an error of 2.8 is shown in Fig. 14a. In contrast, a grid with an error of 0.3 is shown in Fig. 14b. A visual comparison of both figures shows the difference in the linearity of the generated points. The RBFNN was configured using the mentioned error values as the training goal. Except for the error values, the RBFNN hyperparameters for both examples were the same. Observe that, a small training error produces better interpolation results.

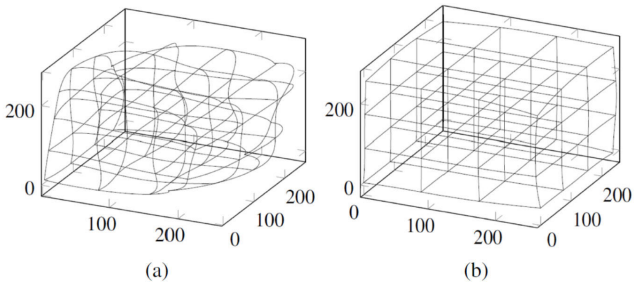

FIGURE 14. Color interpolation results: (a) The grid obtained with an error of 2.8, and (b) The grid obtained with an error of 0.3.

During the execution of the experiments, it was observed that by increasing the color range over an RGB tridimensional space beyond the valid range, the mean color similarity error obtained becomes smaller. However, with values greater than 1000, the RBFNN begins to approximate to its minimum error.

Three different values for n are used in the experiments, 2, 3, and 4. For $n = 2$, there are 35 neurons ($2^3 + 3^3$) in the hidden layer, for $n = 3$, 91 neurons ($3^3 + 4^3$), and for $n = 4$, 189 neurons ($4^3 + 5^3$). The n value defines the number of divisions of the RGB axis for the neuron centers. Several trains and evaluation cycles were applied, using the highest color component values from 255 to 1000 in steps of 50 (the lowest value was always 0), over sets with 27, 60, and 200 pairs of inputs and output samples.

Algorithm 1 Generation of the 3D Grid and Color Error Calculation With the ΔE_{CMC} Method

```
Input: divisions
Output: result
Function RedColorSimilarityError(divisions):
    step ← 255/divisions;
    error ← 0;
    counter ← 0;
    red ← 0;
    green ← 0;
    blue ← 0;
    while green < 255 do
        while blue < 255 do
            while red < 255 do
                color ← Color(red, green, blue);
                estimatedColor ← Net(red, green, blue);
                x ← estimatedColor.red;
                y ← estimatedColor.green;
                z ← estimatedColor.blue;
                Draw3DPoint(x, y, z);
                errorColor = DeltaE_cmc(color, estimatedColor);
                error ← error + errorColor;
                counter ← counter + 1;
                red ← red + 1;
                blue ← blue + step;
                green ← green + step;
            end
        end
    end
    result ← error/counter;
    return result;
End Function
```

Figure 15 shows three examples of how the mean error for the color similarity changes when both the number of neurons in the hidden layer and the distance of the centers over the color range (horizontal axis) changed. A network with few neurons in the hidden layer (n=2) produces a smaller error than models with higher number of neurons (n=4). Also, the RBFNN converges faster, the curve for $n = 2$ is the lowest in the three plots. It is also noticeable that the error decreases when the center dispersion increases. When the dispersion value goes towards 1000, the three curves begin to converge to the same minimum. However, the curve for ($n = 2$) has reached the minimum error when the dispersion is near to 700, as shown in Fig. 15a and 15b.

Training the RBFNN with a set of 200 values produced an error smaller than the one obtained using sets with

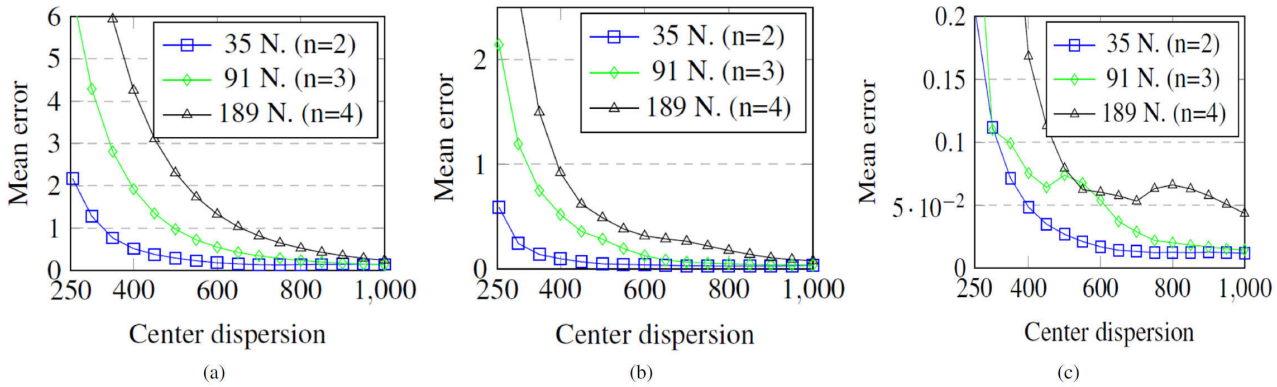

FIGURE 15. The mean color similarity error obtained using: (a) 27, (b) 60, and (c) 200 samples.

27 and 60 values. However, the network presented convergence problems for a higher number of neurons, as shown in Fig. 15c. Also, the time required to train the network increased significantly. The actual timeout was set to 33 minutes for a target error of 0.01. Increasing the timeout to allow lower convergence error is not worthy of the training time. An error of 1 is the threshold to accept two colors as identical. The training was carried out in a Dell workstation with an Intel i7 processor running at 3.0 Mhz, with 8Gb of RAM, no GPU was used.

A set of 60 samples, with $n = 2$, and a dispersion of 700 yielded the best results, with a low color similarity error.

B. CONVERSION FROM RGB TO CIE 1931 xyY

The second experiment was conducted using the same setup of the experiment one and was designed to evaluate the capability to perform the conversion from RGB values measured with a camera to CIE 1931 xyY. The 10 images measured, but not included in the training set, were loaded in the LCD and captured with the camera. The RGB values were fed to the RBFNN, obtaining at the output the values in the xyY space. These values were compared against the values measured with the spectroradiometer.

The results were evaluated for the three estimated elements, luminance (Y) and chromaticity coordinates (x and y). The main difference between the measurements, with the spectroradiometer and the camera, is that the spectroradiometer gives the color value for a localized point on the screen, while the proposed method performs its operation over the 60% of the display area.

In order to have more similar measurements, the nine measures obtained with the spectroradiometer were averaged together. It is important to consider that each of the nine individual measurements does not produce the same value. That means, that the values obtained consist of two elements, a measurement center point and data dispersion. The first one is represented by the average and the second one by the standard deviation. The evaluation was performed against a range of values to include the dispersion of the measurements in the different nine locations. The range was obtained by applying the six-sigma methodology used in manufacturing to define the natural limits in a process, using several measurements over the same product, with the same instrument.

The six-sigma limits for a process, with normal distribution, mean that 99.99966% of the produced parts are inside the limits. This is a standard technique used in manufacture to set the pass/fail criteria for an under control process. The application of the proposed method is intended to be used in a manufacturing process, and this makes valid the application of the six-sigma methodology to calculate the limits to evaluate the result.

The second and third columns in Table 4 show the mean value (μ) and the standard deviation (σ) for the measurements of the nine averaged points shown in Fig. 7. The fourth and fifth columns are the limits calculated by subtracting and adding σ multiplied by 6 to μ. The sixth column is the luminance obtained with the RBFNN, and the seventh column is number of sigmas that the luminance is far from the mean. The underlined values indicate that the result is not inside the six-sigma limits. The same structure was used to create Table 5 for x and Table 6 for y color components.

TABLE 4. Luminance measurements on the 9 points for each pattern sample.

Pattern sample	Reference		Limits		RBFNN result	Sigmas range
	μ	σ	$\mu - 6\times\sigma$	$\mu + 6\times\sigma$		
1	134.0000	3.8630	110.8222	157.1778	134.9883	1
2	176.3000	4.0728	151.8634	200.7367	167.6813	3
3	157.0200	3.8551	133.8893	180.1507	161.9593	2
4	75.7100	1.6460	65.8339	85.5861	66.4392	6
5	32.2778	0.8053	27.4460	37.1096	31.0763	2
6	95.1456	2.3875	80.8205	109.4707	99.5908	2
7	76.5956	2.1756	63.5418	89.6494	74.7269	1
8	6.3810	0.3109	4.5156	8.2464	**3.2839**	10
9	169.1000	4.4133	142.6200	195.5800	170.3235	1
10	75.0600	2.1518	62.1491	87.9709	73.4386	1

From the 30 values shown in Tables 4-6, only 2 were outside the expected range, 1 for the luminance, (see Table 4) and 1 for the y color component (Table 6). That represents about 6.6% of misses. However, about 77% are inside three sigmas, which means that most of the measurements are closer to the

TABLE 5. *x* measurements on the 9 points for each pattern sample.

Pattern sample	Reference		Limits		RBFNN result	Sigmas range
	μ	σ	$\mu - 6 \times \sigma$	$\mu + 6 \times \sigma$		
1	0.2796	0.0018	0.2688	0.2904	0.2738	4
2	0.2643	0.0036	0.2429	0.2857	0.2638	1
3	0.2186	0.0024	0.2040	0.2332	0.2178	1
4	0.2461	0.0045	0.2194	0.2728	0.2496	1
5	0.2160	0.0024	0.2018	0.2302	0.2284	6
6	0.2981	0.0060	0.2621	0.3341	0.2889	2
7	0.3504	0.0028	0.3335	0.3673	0.3378	5
8	0.2956	0.0034	0.2752	0.3160	0.2860	3
9	0.4245	0.0044	0.3981	0.4509	0.4222	1
10	0.3697	0.0031	0.3510	0.3885	0.3734	2

TABLE 6. *y* measurements on the 9 points for each pattern sample.

Pattern sample	Reference		Limits		RBFNN result	Sigmas range
	μ	σ	$\mu - 6 \times \sigma$	$\mu + 6 \times \sigma$		
1	0.5154	0.0061	0.4791	0.5517	0.5118	1
2	0.3275	0.0076	0.2817	0.3733	0.3226	1
3	0.3265	0.0086	0.2751	0.3779	0.3254	1
4	0.1985	0.0047	0.1703	0.2267	0.1972	1
5	0.3262	0.0087	0.2739	0.3785	0.3480	3
6	0.2170	0.0047	0.1888	0.2452	0.2094	2
7	0.5346	0.0042	0.5093	0.5599	0.5246	3
8	0.5270	0.0112	0.4601	0.5939	**0.3560**	16
9	0.5079	0.0040	0.4840	0.5318	0.5068	1
10	0.5729	0.0029	0.5553	0.5905	0.5891	6

mean value than to the value in the limits. In other words, the probability that the measured values with the RBFNN are inside the tolerance is high (93.3%).

The values outside the limits were obtained for the pattern sample number 8, which has the lowest luminance value. Thus, the values for which the RBFNN failed to meet the tolerance were taken when the display intensity was the lowest.

C. DISCUSSION

The results obtained with our proposal were competitive with the results shown in Table 1. In the works by [11], [13], [16], a significant quantity of time was spent into manual camera calibration, parameter adjustments, and establishing lighting conditions. However, our proposal automatically compensates for environmental conditions. Moreover, in the previous work, different measures were employed to determine the color differences. Nevertheless, none of the cited works obtained differences below two units, which means that the colors obtained with our proposal cannot be visually differentiated.

Only the work by Bang-iam *et al.* [13] uses a neural network trained with the backpropagation algorithm for colorimetry purposes and no justification about the network topology was offered. In our work, we explained how to determine the architecture of the RBFNN. Furthermore, we used the RBFNN to predict the CIE values, while the other work used the backpropagation to estimate protein concentrations. Therefore, no comparisons could be carried out.

One of the main differences with the work presented in the literature is that our proposal was implemented in a real automotive scenario. Our results comply with the six-sigma standard, and 77% of the measures are inside three-sigma and 93.3% inside six-sigma. Also, our RBFNN was implemented in a computer with average features, while the other work was implemented using powerful equipment. Moreover, our proposal presented two experiments: color space reconstruction and color prediction.

The selection of the 70 random images, for the measurement experiment, did not produce a uniform population for the RGB color space range. After the RBFNN was trained, it was discovered that missing values, in some parts of the color range, produced a bigger variation for the interpolation of values in some regions. In future experiments, the selection of the color samples will be designed to include color images at the borders and corners of the three-dimensional color space to improve the network performance. It is expected that training the network with those boundary samples will improve the capability to interpolate values with fewer errors.

The failure of the camera to provide a better measurement for the sample patterns with low intensity, can be attributed to the camera configuration, sensitivity, and lens aperture. The camera was adjusted considering the highest intensity patterns to avoid the saturation of the imaging sensor. Therefore, the patterns with low intensity were affected. To solve this problem, it is possible to apply one of the next two solutions:

1) Change the lens aperture and camera gain to be more sensitive to low-intensity images.
2) Use a second camera, adjusted to images with low intensity, using a second RBFNN trained with this camera configuration.

Finally, because most of the points were inside or close to the low or high measurement, it is assumed that the RBFNN can provide a good approximation. However, the RBFNN still needs to be improved to obtain more consistent results. More training samples, with a better distribution over the RGB color space, may increase accuracy.

V. CONCLUSION

This paper presented the application of an RBFNN used for the evaluation of image color quality displayed on LCDs, using a digital camera. In addition to convert the RGB values to the CIExyY, the RBFNN applies corrections to the deformations introduced by the camera position, the lens, and the camera parameters, making possible to compare the measurements with the camera against design specifications measured with a spectroradiometer.

The experiment to test the RBFNN capability to interpolate the RGB color space showed that the training set should include values at the borders (color axis) and corners to achieve better results. The training samples for the color conversion showed large errors for colors in some areas of the 3D space. This failure is attributed to the lack of training points in some 3D RGB color space regions. However, for the conversion from RGB to CIExyY an accuracy of 93.3% was obtained.

In future evaluations, the training samples will be artificially distributed to include values at the corners and the color axis to improve the color conversion. Also, it will be

desirable to test other neural network architectures, including deep neural networks.

REFERENCES

[1] H. Chen, J. Lee, B. Lin, S. Chen, and S. Wu, "Liquid crystal display and organic light-emitting diode display: Present status and future perspectives," *Light, Sci. Appl.*, vol. 7, pp. 1–13, Mar. 2018.
[2] P. Knoll, *Handbook of Visual Display Technology*. Cham, Switzerland: Springer, 2016.
[3] H. Hayase and S. Wu, *Automotive Display Market Tracker-2017*. London, U.K.: IHS Markit, 2017.
[4] K. Blankenbach, "Advanced automotive display measurements: Selected challenges and solutions," *J. Soc. Inf. Display*, vol. 26, no. 9, pp. 517–525, Sep. 2018.
[5] T. Uchida, "40 years research and development on liquid crystal displays," *Jpn. J. Appl. Phys.*, vol. 53, pp. 1–6, Feb. 2014.
[6] H. Kim, H. Gu, Y.-H. Kim, K.-A. Choi, and S.-J. Ko, "A novel quality assessment method for flat panel display defects," *J. Display Technol.*, vol. 12, no. 5, pp. 500–505, May 2016.
[7] S. Jin, C. Ji, C. Yan, and J. Xing, "TFT-LCD mura defect detection using DCT and the dual-γ piecewise exponential transform," *Precis. Eng.*, vol. 54, pp. 371–378, Oct. 2018.
[8] S.-H. Huang and Y.-C. Pan, "Automated visual inspection in the semiconductor industry: A survey," *Comput. Ind.*, vol. 66, pp. 1–10, Jan. 2015.
[9] G. Nam, H. Lee, S. Oh, and M. H. Kim, "Measuring color defects in flat panel displays using HDR imaging and appearance modeling," *IEEE Trans. Instrum. Meas.*, vol. 65, no. 2, pp. 297–304, Feb. 2016.
[10] J. Lin and Y. Chiang, "A novel method for testing LCD by integrating shorting bar and Taguchi doe technologies," *J. Mar. Sci. Technol.*, vol. 24, pp. 539–547, Jun. 2016.
[11] P. Notermans and N. Cohen, "Next-generation metrology facilitates next-generation displays," *Inf. Display*, vol. 32, no. 6, pp. 24–28, Nov. 2016.
[12] A. Corning, "Matching human visual perception," *Qual. Mag.*, vol. 1, pp. 1–8, Jul. 2018.
[13] N. Bang-Iam, Y. Udnan, and P. Masawat, "Design and fabrication of artificial neural network-digital image-based colorimeter for protein assay in natural rubber latex and medical latex gloves," *Microchemical J.*, vol. 106, pp. 270–275, Jan. 2013.
[14] M. Lutfi, A. Aprian, N. Meileza, M. Hitsmi, R. Elvia, L. Rahmidar, and A. Khaydarov, "Smartphone coupled with a paper-based colorimetric device for sensitive and portable mercury ion sensing," *Chemosensors*, vol. 7, pp. 1–9, Jun. 2019.
[15] A. Silva and F. Rocha, "A novel approach to detect milk adulteration based on the determination of protein content by smartphone-based digital image colorimetry," *Food Control*, vol. 115, pp. 1–6, Sep. 2020.
[16] P. Sanmartín, E. Chorro, D. Vázquez-Nion, F. M. Martínez-Verdú, and B. Prieto, "Conversion of a digital camera into a non-contact colorimeter for use in stone cultural heritage: The application case to Spanish granites," *Measurement*, vol. 56, pp. 194–202, Oct. 2014.
[17] A. P. Markopoulos, S. Georgiopoulos, and D. E. Manolakos, "On the use of back propagation and radial basis function neural networks in surface roughness prediction," *J. Ind. Eng. Int.*, vol. 12, no. 3, pp. 389–400, Sep. 2016.
[18] M. Kumar and N. Yadav, "Multilayer perceptrons and radial basis function neural network methods for the solution of differential equations: A survey," *Comput. Math. Appl.*, vol. 62, no. 10, pp. 3796–3811, Nov. 2011.
[19] V. Agarwal and S. Bhanot, "Radial basis function neural network-based face recognition using firefly algorithm," *Neural Comput. Appl.*, vol. 30, no. 8, pp. 2643–2660, Oct. 2018.
[20] H. Yu, T. Xie, S. Paszczynski, and B. M. Wilamowski, "Advantages of radial basis function networks for dynamic system design," *IEEE Trans. Ind. Electron.*, vol. 58, no. 12, pp. 5438–5450, Dec. 2011.
[21] C. Juliani and S. Ellefmo, "Prospectivity mapping of mineral deposits in Northern Norway using radial basis function neural networks," *Minerals*, vol. 9, pp. 1–15, Feb. 2019.
[22] C. S. K. Dash, A. K. Behera, S. Dehuri, and S.-B. Cho, "Building a novel classifier based on teaching learning based optimization and radial basis function neural networks for non-imputed database with irrelevant features," *Appl. Comput. Informat.*, vol. 1, pp. 1–7, Aug. 2020.
[23] D. Kriesel. (2018). *A Brief Introduction to Neural Networks*. Accessed: Mar. 20, 2020. [Online]. Available: http://www.dkriesel.com
[24] T. Steinel and M. Wolf, "Bringing true colors to MicroLED displays," *Inf. Display*, vol. 36, no. 3, pp. 19–23, May 2020.
[25] I. Tomić, S. Dedijer, D. Novakovikć, and A. Hladnik, "Camera characterization for colorimetric assessment of goniochromatic prints," *J. Imag. Sci. Technol.*, vol. 61, pp. 1–15, Mar. 2017.
[26] I. Guyon and A. Elisseeff, "An introduction to variable and feature selection," *J. Mach. Learn. Res.*, vol. 3, pp. 1157–1182, Jan. 2003.
[27] G. Diaz, A. Kokoue-Nkoutche, G. Nannicini, and H. Samulowitz, "An effective algorithm for hyperparameter optimization of neural networks," *IBM J. Res. Develop.*, vol. 61, pp. 1–11, Sep. 2017.
[28] F. J. Pontes, G. F. Amorim, P. P. Balestrassi, A. P. Paiva, and J. R. Ferreira, "Design of experiments and focused grid search for neural network parameter optimization," *Neurocomputing*, vol. 186, pp. 22–34, Apr. 2016.
[29] J. M. Soto-Hidalgo, D. Sánchez, J. Chamorro-Martínez, and P. M. Martínez-Jiménez, "Color comparison in fuzzy color spaces," *Fuzzy Sets Syst.*, vol. 390, pp. 160–182, Jul. 2020.
[30] D. Durmus, "CIELAB color space boundaries under theoretical spectra and 99 test color samples," *Color Res. Appl.*, vol. 45, no. 5, pp. 796–802, Oct. 2020.
[31] W. Mokrzycki and M. Tatol, "Colour difference ΔE—A survey," *Mach. Graph. Vis.*, vol. 20, pp. 383–411, Apr. 2011.

FELIPE ARIAS DEL CAMPO was born in Durango, Mexico, in 1970. He received the B.S. degree in computer sciences engineering from the Instituto Tecnológico de Chihuahua II, in 1993, and the M.Sc. degree in electrical engineering, in 2016. He is currently pursuing the Ph.D. degree with the Universidad Autónoma de Ciudad Juarez. During the bachelor's degree he participated on the national congress CONAISCO in 1991, 1992, and 1993, as a Speaker on Graphics and Artificial Intelligence areas. From 1993 to 1997, he was a Computer Science Cathedra Professor with the Instituto Tecnológico de Chihuahua II and the Instituto Tecnológico de Delicias. Since 2005, he has been working with the Automotive Industry as a Manufacturing Technology Engineer on projects related to automotive communication protocols, manufacturing quality and statistical tools development, computer vision and image processing, cybersecurity, continuous improvement, and technology support, working with the different manufacturing sites and different technical centers in the USA, Europe, and Asia. He is the author of several software tools used as standard applications for Aptiv world-wide, winning three global awards for its contribution. His research interests include software development, statistical analysis, computer vision, image analysis, deep learning, cryptography, data visualization, serial protocols, and 3D modeling.

OSSLAN OSIRIS VERGARA VILLEGAS (Senior Member, IEEE) was born in Cuernavaca, Morelos, Mexico, on July 3, 1977. He received the B.S. degree in computer engineering from the Instituto Tecnologico de Zacatepec, Mexico, in 2000, the M.Sc. degree in computer science from the Center of Research and Technological Development (CENIDET), in 2003, and the Ph.D. degree in computer science from CENIDET, in 2006. He is currently working as a Professor with the Universidad Autónoma de Ciudad Juárez, Chihuahua, Mexico, where he is the Head of the Computer Vision and Augmented Reality Laboratory. He is also a Level One Member of the Mexican National Research System. He has coauthored more than 100 book chapters, journals, and international conference papers. He has directed more than 50 B.S., M.Sc., and Ph.D. thesis. His research interests include pattern recognition, digital image processing, augmented reality, and mechatronics. He is a Senior Member of the IEEE Computer Society and a Mexican Computing Academy Member. He also serves as an Editorial Board Member and a Reviewer for several peer-reviewed international journals and conferences.

VIANEY GUADALUPE CRUZ SÁNCHEZ was born in Cárdenas, Tabasco, México, on September 14, 1978. She received the B.S. degree in computer engineering from the Instituto Tecnológico de Cerro Azul, México, in 2000, the M.Sc. degree in computer science from the Center of Research and Technological Development (CENIDET), in 2004, and the Ph.D. degree in computer science from CENIDET, in 2010. She currently works as a Professor with the Autonomous University of Ciudad Juarez, Chihuahua, México. Her research interests include neuro symbolic hybrid systems, digital image processing, knowledge representation, artificial neural networks, and augmented reality. She is a member of the IEEE Computer Society.

HUMBERTO DE JESÚS OCHOA DOMÍNGUEZ (Member, IEEE) received the B.Eng. degree in industrial electronics from the Technological Institute of Veracruz, México, the M.Sc. degree in electronics from the Technological Institute of Chihuahua, México, and the Ph.D. degree in electrical engineering from the University of Texas at Arlington, USA. He worked as an Electronics Officer with Mexican Merchant Marine. He is currently with the Department of Ingeniería Eléctrica y Computación, Universidad Autónoma de Ciudad Juárez, Mexico. His current teaching and research interests include multirate systems for medical image analysis, image restoration and reconstruction, image and video coding, statistical signal processing, and pattern recognition.

MANUEL NANDAYAPA (Member, IEEE) received the B.S. degree in electronics engineering from the Institute of Technology of Tuxtla Gutierrez, Mexico, in 1997, the M.S. degree in mechatronics engineering from CENIDET, Mexico, in 2003, and the Ph.D. degree (Engineering) in energy and environmental science from the Nagaoka University of Technology, Japan, in 2012. He is currently with the Department of Industrial and Manufacturing Engineering, Universidad Autónoma de Ciudad Juárez. His research interests include mechatronics, motion control, and haptic interfaces.